http://informahealthcare.com/xen
ISSN: 0049-8254 (print), 1366-5928 (electronic)

Xenobiotica

Xenobiotica, Early Online: 1–13
 DOI: 10.3109/00498254.2015.1047812

informa
healthcare

RESEARCH ARTICLE

Metabolism of the anthelmintic drug niclosamide by cytochrome P450 enzymes and UDP-glucuronosyltransferases: metabolite elucidation and main contributions from CYP1A2 and UGT1A1

Danyi Lu*, Zhiguo Ma*, Tianpeng Zhang, Xingwang Zhang, and Baojian Wu

Division of Pharmaceutics, College of Pharmacy, Jinan University, Guangzhou, P.R. China

Abstract

1. Niclosamide is an old anthelmintic drug that shows potential in fighting against cancers. Here, we characterized the metabolism of niclosamide by cytochrome P450 enzymes (CYPs) and UDP-glucuronosyltransferases (UGTs) using human liver microsomes (HLM) and expressed enzymes.
2. NADPH-supplemented HLM (and liver microsomes from various animal species) generated one hydroxylated metabolite (M1) from niclosamide; and UDPGA-supplemented liver microsomes generated one mono-*O*-glucuronide (M2). The chemical structures of M1 (3-hydroxy niclosamide) and M2 (niclosamide-2-*O*-glucuronide) were determined through LC–MS/MS and/or NMR analyses.
3. Reaction phenotyping revealed that CYP1A2 was the main enzyme responsible for M1 formation. The important role of CYP1A2 in niclosamide metabolism was further confirmed by activity correlation analyses as well as inhibition experiments using specific inhibitors.
4. Although seven UGT enzymes were able to catalyze glucuronidation of niclosamide, UGT1A1 and 1A3 were the enzymes showed the highest metabolic activities. Activity correlation analyses demonstrated that UGT1A1 played a predominant role in hepatic glucuronidation of niclosamide, whereas the role of UGT1A3 was negligible.
5. In conclusion, niclosamide was subjected to efficient metabolic reactions hydroxylation and glucuronidation, wherein CYP1A2 and UGT1A1 were the main contributing enzymes, respectively.

Keywords

CYP, glucuronidation, hydroxylation, niclosamide, reaction phenotyping, UGT

History

Received 28 March 2015
Revised 29 April 2015
Accepted 30 April 2015
Published online 11 June 2015

Introduction

Poor pharmacokinetic property is one of the main causes to the high rate of drug attrition (Kola & Landis, 2004; Prentis et al., 1988). Drug metabolism, an indispensable component of pharmacokinetics, is a main determinant to the drugability of lead compounds (Costa et al., 2014). Extensive metabolism tends to result in fast drug clearance (and very short half-life), low bioavailability and therapeutic failures, whereas poor (or undesired) metabolism would lead to drug accumulation (in off-target tissues) and side effects. Knowing the enzymes involved in the metabolism of a drug is also useful in predicting variability (e.g. if the enzymes are polymorphic) and potential drug–drug interactions with co-administered drugs (or herbal remedies). Hence, it is of great importance to determine the metabolic profiles and to establish the relationships between metabolism and efficacy/toxicity for drugs and drug candidates.

Drug metabolism is classified into phase I and phase II metabolism. Phase II metabolism (conjugation) often occur on metabolites produced by phase I oxidation but does occur directly on parent drugs bearing appropriate functional moieties such as hydroxyl group and carboxylic acid. Cytochrome P450 enzymes (CYPs) are the principal phase I enzymes that catalyze the oxidation and reduction reactions. CYP enzymes are classified into 17 families and 39 subfamilies; the main enzymes contributing to drug metabolism are often from the CYP1, 2 and 3 families, including CYP1A2, 1B1, 2A6, 2C8, 2C9, 2C19, 2D6, 2E1 and 3A4 (Ortiz de Montellano, 2005). UDP-glucuronosyltransferases (UGTs) mediated glucuronidation is responsible for clearance of 35% of drugs that are metabolized by phase II enzymes (Evans & Relling, 1999). The glucuronidation reaction occurs via transfer of a glucuronic acid moiety to the substrates (Wells et al., 2004). In humans, UGT enzymes are divided into four families, UGT1, UGT2, UGT3 and UGT8 (Mackenzie et al., 2005). Enzymes from UGT1A (with nine members) and 2B families (with seven members) are the main contributors to

*These authors contributed equally to this work.

Address for correspondence: Baojian Wu, Ph.D., Division of Pharmaceutics, College of Pharmacy, Jinan University, 601 Huangpu Avenue West, Guangzhou 510632, P.R. China. E-mail: bj.wu@hotmail.com

xenobiotic/drug metabolism. It has been reported that the CYP and UGT enzymes in total contribute to metabolism of over 80% clinical drugs (Emoto et al., 2010). Therefore, it is of great value to characterize the metabolism of drugs (and drug candidates) by both CYPs and UGTs in humans.

The anthelmintic drug niclosamide has been used in management of tapeworm infections for half a century (Al-Hadiya, 2005). Niclosamide kills tapeworms through inhibition of oxidative phosphorylation and stimulation of adenosine triphosphatese activity in the mitochondria (Al-Hadiya, 2005). In recent years, niclosamide has been identified as a potential anticancer agent (Li et al., 2014; Pan et al., 2012). The mechanisms for its anticancer action appear to be rather complex. Niclosamide inhibits multiple signaling pathways that regulate cancer progression such as the mTORC1 (Fonseca et al., 2012), NF-κB (Jin et al., 2010), and Notch pathways (Wang et al., 2009). It also induces cell cycle arrest, growth inhibition and apoptosis by targeting mitochondria (Park et al., 2011). Moreover, niclosamide shows strong inhibitory effects on the growth of cancer stem cells (Jin et al., 2010; Li et al., 2014; Pan et al., 2012). It is also noted that niclosamide is an effective bacterial killer against *Pseudomonas aeruginosa* (Imperi et al., 2013).

Oral niclosamide is well tolerated in humans and animals (Al-Hadiya, 2005). The good tolerability may be accounted for by limited oral absorption of the drug (Al-Hadiya, 2005). The exact reasons are unknown as to why niclosamide is poorly bioavailable after oral uptake. Poor water solubility may be a limiting factor to intestinal absorption of niclosamide (Pan et al., 2012). In an early study, a reduced metabolite was generated from niclosamide by mouse and sheep liver homogenates (Douch & Gahagan, 1977). In a latter study, the glucuronidated and sulfate metabolites were found in fishes (Dawson et al., 1999) and rats (Griffiths & Facchini, 1979) after exposure to niclosamide. However, no specific data for metabolism of niclosamide in humans are available in the literature.

Niclosamide is old anthelmintic drug that also shows potential in fighting against cancers and bacteria (Imperi et al., 2013; Li et al., 2014). In the present study, we aimed to characterize the metabolism of niclosamide by cytochrome P450 enzymes (CYPs) and UGTs using human liver microsomes (HLM) and expressed enzymes. The chemical structures of metabolites were identified through LC–MS/MS and/or NMR analyses. Screening of the enzymes with metabolic activities toward niclosamide was performed using commercially available expressed enzymes (CYPs and UGTs). Reaction phenotyping, activity correlation analysis and/or inhibition experiments with specific inhibitors were employed to determine the main enzymes contributing to hepatic metabolism of niclosamide. Our study for the first time revealed that niclosamide was subjected to efficient hydroxylation and glucuronidation, wherein CYP1A2 and UGT1A1 were the main contributing enzymes, respectively.

Materials and methods

Materials

Expressed human CYP enzymes (CYP1A1, 1A2, 1B1, 2B6, 2C8, 2C9, 2C19, 2D6, 2E1, 3A4 and 3A5), UGT enzymes (UGT1A1, 1A3, 1A4, 1A6, 1A7, 1A8, 1A9, 1A10, 2B4, 2B7, 2B15 and 2B17), pooled HLM, dog liver microsomes (DLM), monkey liver microsomes (cynomolgus, MkLM), mouse liver microsomes (MsLM), mini-pig liver microsomes (PLM), rat liver microsomes (RLM) and fulvoxamine maleate were purchased from BD Biosciences (Woburn, MA). Niclosamide (purity >99%) was purchased from Xiya Chemical Technology Co. Ltd. (Chengdu, China). β-Nicotinamide adenine dinucleotide 2′-phosphate reduced tetrasodium salt hydrate (NADPH), uridine diphosphoglucuronic acid (UDPGA), alamethicin, D-saccharic-1,4-lactone monohydrate, β-glucuronidase and 17β-estradiol (or β-estradiol) were purchased from Sigma-Aldrich (St. Louis, MO). β-Estradiol 3-glucuronide and chenodeoxycholic acid 24-acyl-glucuronide were purchased from Toronto Research Chemicals (Ontario, Canada). Phenacetin, 4-acetamidophenol, α-naphthoflavone, chenodeoxycholic acid and apigenin were purchased from Aladdin Chemicals (Shanghai, China). Individual HLMs ($n = 14$) obtained from healthy livers were purchased from Rild Research Institute for Liver Diseases (Shanghai, China). All other materials (typically analytical grade or better) were used as received.

In vitro phase I metabolism assay

In vitro phase I metabolism of the test compounds was performed as described (Fang et al., 2014). In brief, the incubation medium (300 µl) contained liver microsomes (or expressed CYP enzymes), $MgCl_2$ (5 mM), NADPH (1 mM) and test compound in 50 mM potassium phosphate (pH 7.4). The reaction was initiated by the addition of NADPH and terminated by adding 75 µl ice-cold acetonitrile at predetermined time points. The samples were vortexed and centrifuged at 18 000*g* for 15 min. The supernatant was collected and subjected to analysis by HPLC or UPLC-QTOF/MS. All experiments were performed in triplicate. Control incubations were performed without the cofactor NADPH. In all experiments, niclosamide was dissolved in ethanol to obtain a 10 mM stock solution and serially diluted to the required concentrations with ethanol. The percentage of organic solvent in the incubation system did not exceed 1%. Preliminary experiments were performed to ensure that the metabolic rates were determined under linear conditions with respect to incubation time and protein concentration. The exact concentrations of niclosamide and the incubation time for rate determination can be found in Table S1 (Supplementary Materials).

Glucuronidation assay

The test compounds were incubated with liver microsomes (or expressed UGT enzymes) to determine the rates of glucuronidation as described in our previous publication (Liu et al., 2014a). In brief, the incubation medium (300 µl) contained microsomes, $MgCl_2$ (0.88 mM), saccharolactone (4.4 mM), alamethicin (22 µg/ml), UDPGA (3.5 mM) and test compound in 50 mM potassium phosphate (pH 7.4). The reaction was initiated by incubation at 37 °C and terminated by adding 75 µl ice-cold acetonitrile, followed by vortex and centrifugation (15 min; 18 000*g*). The supernatant was subjected to analysis by HPLC and/or UPLC-QTOF/MS. Control incubations were performed without UDPGA. All experiments were performed in triplicate. Preliminary

experiments were performed to ensure that the rates of glucuronidation were determined under linear conditions with respect to incubation time and protein concentration. The exact concentrations of niclosamide and the incubation time for determination of glucuronidation rates can be found in Table S2 (Supplementary Materials).

To confirm formation of *O*-glucuronide, hydrolysis of the metabolite in the incubation was performed using β-glucuronidase. The metabolite in incubation medium was generated according to the glucuronidation assay protocol. Subsequently, the incubation mixture was subjected to purification using solid phase extraction (SPE, Suplclean™ LC-C18, Supelco Inc., Bellefone, PA) as described (Sun et al., 2014). The purified sample from SPE (containing both parent compound and glucuronide) was incubated with β-glucuronidase (25 U). After 20 min (sufficient for complete hydrolysis of glucuronide), 50 µl ice-cold acetonitrile was added to the incubation medium, followed by vortex and centrifugation (15 min; 18 000*g*). The supernatant was analyzed by HPLC. Control experiment was performed in the absence of β-glucuronidase.

Structural identification of niclosamide metabolites by UPLC-QTOF/MS and 1H NMR

Structural identification of phase I and UGT metabolites was performed using UPLC-QTOF/MS. Chromatographic separation was performed using the Waters ACQUITY UPLC system and BEH column (2.1 mm × 50 mm, 1.7 µm; Waters, Milford, MA). Elution was performed using a gradient of formic acid (0.1%) in water (mobile phase A) versus formic acid (0.1%) in acetonitrile (mobile phase B) at a flow rate of 0.45 ml/min. The gradient elution program was 10% B at 0–1 min, 10 to 95% B at 1–3 min and 95 to 10% B at 3.5–4 min. Mass spectrometry analysis was performed on the Xevo G2 Q-TOF/MS (Waters) using the electrospray ionization source (negative ion mode) as described (Liu et al., 2014b). A collision energy of 20 eV was used for MS/MS scanning.

A large amount of phase I metabolite M1 was generated according to the *in vitro* incubation protocol except for that the incubation volume was scaled up to 500 ml. In brief, niclosamide (25 µM) was incubated with PLM (final protein concentration, 0.25 mg/ml), 5 mM $MgCl_2$ and 1 mM NADPH. After incubation for 8 h, ice-cold acetonitrile (50 ml) was added to precipitate the proteins. The incubation mixture was centrifuged at 18 000 *g* for 15 min. The supernatant was concentrated and injected to HPLC system. Niclosamide and its metabolite M1 were separated by the Agilent TC-C18(2) column (5 µm, 4.6 mm × 250 mm) using 75% acetonitrile–0.1% formic acid in water as the mobile phase. Fractions containing M1 were collected and dried i*n vacuo*. The purity of M1 was about 99% by HPLC-UV analysis. The purified metabolite (M1) was dissolved in dimethyl sulfoxide-d_6 (Euriso-Top, Saint-Aubin, France) for NMR analysis. ^{1}H NMR spectra of M1 were recorded on Bruker AV-500 spectrometer (Bruker, Rheinstetten, Germany) using tetramethylsilane as an internal standard.

Kinetic evaluation

The rates of metabolite formation were determined for niclosamide at a series of concentrations according to the *in vitro* metabolism assay protocols. The kinetic model, Michaelis–Menten (Equation 1) or biphasic equation (Equation 2) or substrate inhibition equation (Equation 3) or Hill equation (Equation 4), was fitted to the data of formation rates versus substrate concentrations. Model selection was based on visual inspection of the characteristic Eadie–Hofstee plots (Hutzler & Tracy, 2002). Model fitting and parameter estimation were performed using the Graphpad Prism V5 software (San Diego, CA).

$$V = \frac{V_{max} \times [S]}{K_m \times [S]}, \quad (1)$$

$$V = \frac{V_{max\,1} \times [S]}{K_{m1} \times [S]} + \frac{V_{max\,2} \times [S]}{K_{m2} \times [S]}, \quad (2)$$

$$V = \frac{V_{max} \times [S]}{K_m \times [S] \times (1 + ([S]/K_{si}))}, \quad (3)$$

$$V = \frac{V_{max} \times [S]^n}{S_{50}^n + [S]^n}, \quad (4)$$

where V is the rate of reaction, V_{max} is the maximal velocity, K_m is the Michaelis constant, K_{si} is the substrate inhibition constant, S_{50} is the substrate concentration resulting in 50% of V_{max} and n is the Hill coefficient. The intrinsic clearance (CL_{int}) was derived by V_{max}/K_m and the maximal clearance (CL_{max}) for the Hill equation model was obtained using Equation (5).

$$CL_{max} = \frac{V_{max}}{S_{50}} \times \frac{n-1}{n(n-1)^{1/n}}. \quad (5)$$

Quantification of drugs and their metabolites

Quantification of niclosamide and its metabolites were performed with the HPLC system (Dionex Ultimate 3000 series, Thermo Scientific, Waltham, MA) consisting of a quaternary pump, a degasser, an autosampler, a column heater and a multichannel rapid scanning UV–Vis detector. Niclosamide and its metabolites were separated by an Agilent TC-C18(2) column (5 µm, 4.6 mm × 250 mm) guarded with a precolumn at 40 °C. The injection volume was set to be 20 µl and the flow rate was 1.0 ml/min. It was noted that different gradient programs were applied in analyses of 3-hydroxy niclosamide (M1) and niclosamide 2-glucuronide (M2). Due to the lack of reference standard for M2, quantification of M2 was based on the standard curve of the parent drug (niclosamide) and further calibrated using the correction factor. The correction factor ($K = 1.03$) was derived exactly as described (Sun et al., 2014). The analytical methods were validated with respect to linearity (9.8–5000 nM), precision (RSD <5%) and accuracy (95–105%). The lower limits of quantification for M1 and M2 were 0.021 and 0.018 µM, respectively. No matrix effects were detected for both metabolites.

Concentrations of phenacetin and its metabolite 4-acetamidophenol were also determined with the same HPLC system. Detailed analytical conditions are summarized

in Table S3 (Supplemental Materials). Concentrations of estradiol and its 3-glucuronide in microsomal incubations were determined by Waters ACQUITY UPLC system. Concentrations of chenodeoxycholic acid and its 24-acyl-glucuronides were determined by the UPLC-QTOF/MS system consisting of Waters ACQUITY UPLC and Xevo G2 QTOF/MS. Analyte quantification using the UPLC-QTOF/MS method has been described in our previous publications (Liu et al., 2014a,b). Detail analytical conditions are summarized in Table S3.

Activity correlation analysis

The metabolic activities of individual HLMs ($n = 14$) toward niclosamide, phenacetin (a probe substrate for CYP1A2) (Zhou et al., 2009), β-estradiol (a probe substrate for UGT1A1) (Seo et al., 2014) and chenodeoxycholic acid (a probe substrate for UGT1A3) (Seo et al., 2014) were determined, respectively, according to the metabolism assay protocols as described above. Phenacetin (10 μM) was incubated with NADPH-supplemented individual HLM (0.25 mg/ml) for 20 min. Estradiol (20 μM) was incubated with UDPGA-supplemented individual HLM (0.265 mg/ml) for 120 min. Chenodeoxycholic acid (20 μM) was incubated with UDPGA-supplemented individual HLM (0.265 mg/ml) for 60 min. Correlation analyses were performed between niclosamide 3-hydroxylation and phenacetin deethylation, between niclosamide glucuronidation and β-estradiol 3-*O*-glucuronidation, and between niclosamide glucuronidation and chenodeoxycholic acid 24-acyl-glucuronidation. Correlation (Pearson) analysis was performed using GraphPad Prism V5 software.

Chemical inhibition assay

α-Naphthoflavone was used as a CYP1A2 inhibitor in many studies (Reid et al., 1999; Shet et al., 1997; Tassaneeyakul et al., 1993). The natural flavone apigenin showed a potent inhibitory effect on CYP1A2 with an inhibition mechanism similar to α-naphthoflavone (Shimada et al., 2010; von Moltke et al., 2004). Fluvoxamine at low concentrations selectively inhibited the activity of CYP1A2 (Nakajima et al., 1999; Pastrakuljic et al., 1997). To better understand the role of CYP1A2 in hydroxylation of niclosamide in NADPH-supplemented HLM, chemical inhibition studies were performed using the three small-molecule inhibitors fluvoxamine, α-naphthoflavone and apigenin. In brief, niclosamide (2.5 μM) was incubated with NADPH-supplemented HLM (0.25 mg/ml) for 60 min in the presence or absence of an inhibitor (i.e., fluvoxamine at 0.5, 1, 2.5 and 5 μM; α-naphthoflavone at 0.01, 0.1, 0.5 and 1 μM; and apigenin at 0.5, 1, 2 and 5 μM). The inhibitors' stock solutions were prepared in methanol and added into the incubation medium with a dilution ratio of 200.

Statistical analysis

Data are expressed as mean ± SD. The two-tailed Student's *t* test was used to compare the mean difference. The prior level of significance was set at 5% or $p < 0.05$.

Results

Structural elucidation of niclosamide metabolites in microsomal incubations

In the presence of NADPH, HLM, RLM, MsLM, PLM, DLM and MkLM generated one metabolite (M1) only from niclosamide (Figure 1A). Niclosamide formed a deprotonated molecule ($[M-H]^-$) at *m/z* 324.981 in the negative ion scan mode. The metabolite M1 showed an ion at *m/z* 340.973. An increase of 16 Da in mass indicated that M1 was a mono-hydroxylated product. The fragment ions of niclosamide were observed at *m/z* 289.000 and 170.996, whereas those of M1 were observed at *m/z* 304.996 and 170.996 (Figure 1B). Fragmentation pattern analysis of M1 and the parent drug revealed that the site of hydroxylation was located at the aromatic ring of the 5-chlorosalicylic acid group (Figure 1C).

To determine the exact site of hydroxylation, M1 was purified in a sufficient quantity (~5 mg) and then analyzed by ^{1}H NMR (Figure 1C). The signals for the aromatic protons (H-3′, H-5′ and H-6′) in the 2-chloro-4-nitroaniline group were assigned. This was consistent with previous finding that the site of hydroxylation was located at the 5-chlorosalicylic acid portion. Further, another two aromatic protons of δ 6.61 (d, $J = 2.7$ Hz) and 7.16 (d, $J = 2.8$ Hz) at the meta-position were assigned to the H-4 and H-6, respectively. Therefore, M1 was identified as the 3-hydroxylated metabolite of niclosamide (i.e. 3-hydroxy niclosamide).

In the presence of UDPGA, HLM and the liver microsomes from various animal species generated one metabolite (M2) from niclosamide (Figure 2A). M2 formed a deprotonated molecule at *m/z* 501.013 (Figure 2B). An increase of 176 Da in mass indicated that M2 was a glucuronidated metabolite. The fragment ion of M2 was observed at *m/z* 324.982 that corresponded exactly to the ion of niclosamide (Figure 2B). This was additional evidence that M2 was formed by conjugation of a glucuronic acid to the parent drug. Furthermore, β-glucuronidase catalyzed the hydrolysis of M2 back to niclosamide, confirming that *O*-glucuronide was generated (Figure 2C). Generation of a tertiary *N*-glucuronide [i.e. glucuronidation occurring at the secondary amine (=NH) group] was unlikely because the tertiary *N*-glucuronide is resistant to β-glucuronidase hydrolysis (Kassahun et al., 1998).

Reaction kinetics for hydroxylation of niclosamide by liver microsomes

Kinetic profiling revealed that formation of M1 in all liver microsomes except PLM followed the classical Michaelis–Menten kinetics (Figure 3). Hydroxylation mediated by PLM showed a sigmoidal profile that was well modeled by Hill equation (Figure 3F). Niclosamide hydroxylation was the most efficient in HLM with a CL_{int} (intrinsic clearance) value of 22.6 μl/min/mg (Table 1). Marked species differences were noted for the derived kinetic parameters (Table 1). The K_m values of human and monkey were similar (1.38 versus 1.71 μM) and were much lower than those of other species (4.51–6.24 μM) (Table 1). The V_{max} values ranged from 10.4 (MkLM) to 31.2 pmol/min/mg (HLM). The CL_{int} value of human was 22.6 μl/min/mg, a figure much higher than those of other species (2.43–6.88 μl/min/mg) (Table 1).

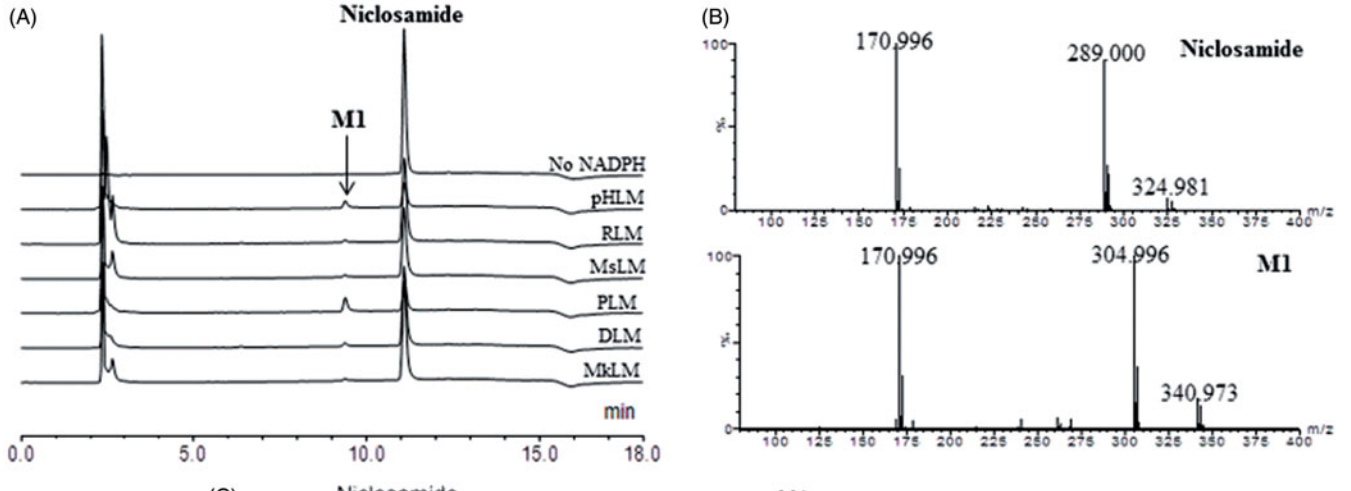

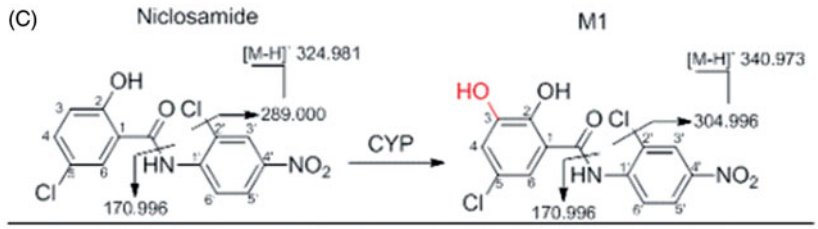

Niclosamide	M1	Assignment
7.10 (d, J = 8.8 Hz, 1H)	-	H-3
7.54 (dd, J = 8.8, 2.8 Hz, 1H)	6.61 (d, J = 2.7 Hz, 1H)	H-4
7.96 (d, J = 2.8 Hz, 1H)	7.16 (d, J = 2.8 Hz, 1H)	H-6
8.29 (dd, J = 9.2, 2.6 Hz, 1H)	8.19 (dd, J = 9.3, 2.7 Hz, 1H)	H-5'
8.43 (d, J = 2.6 Hz, 1H)	8.32 (d, J = 2.7 Hz, 1H)	H-6'
8.81 (d, J = 9.2 Hz, 1H)	8.95 (d, J = 9.3 Hz, 1H)	H-3'

Figure 1. (A) The representative HPLC chromatograms for quantitative analyses of niclosamide and its phase I metabolites in various liver microsomes. (B) MS/MS spectrum of niclosamide and its hydroxylated metabolite M1. (C) Structure, fragmentation pathway and ^{1}H NMR data of niclosamide and its hydroxylated metabolite M1. HLM, human liver microsomes; DLM, dog liver microsomes; PLM, mini-pig liver microsomes; MkLM, monkey liver microsomes; MsLM, mouse liver microsomes; RLM, rat liver microsomes.

Hydroxylation of niclosamide by expressed CYP enzymes

Of tested CYP enzymes (with commercial availability), only CYP1A1 and 1A2 catalyzed hydroxylation of niclosamide (Figure 4A). The metabolic activity of CYP1A2 was 90-fold higher than that of CYP1A1, indicating that CYP1A2 played a predominant role in hydroxylation of niclosamide (Figure 4A). The hydroxylation kinetics of niclosamide by CYP1A2 displayed a substrate inhibition profile (Figure 4B). The low K_m value of 4.88 μM indicated that CYP1A2 was a high-affinity enzyme toward niclosamide (Table 1). The high CL_{int} value of 1.52 ml/min/nmol was suggestive of an efficient hydroxylation mediated by CYP1A2 (Table 1). We were unable to determine the kinetic parameters for CYP1A1 due to its low metabolic activity toward niclosamide.

Activity correlation analyses and inhibition assays for CYP1A2

It is known that CYP1A2 catalyzes metabolism of phenacetin, generating the deethylated product 4-acetamidophenol (Bjornsson et al., 2003). This deethylation reaction of phenacetin has been widely accepted as a functional marker for CYP1A2. We determined the metabolic activities of individual HLM ($n = 14$) toward phenacetin and niclosamide, respectively. It was found that niclosamide hydroxylation was strongly correlated with phenacetin deethylation ($r = 0.876$; $p < 0.001$) (Figure 4C), indicating that CYP1A2 played an important role in metabolism of niclosamide in the liver.

All three chemical inhibitors (i.e., fluvoxamine, α-naphthoflavone and apigenin) showed significant inhibitory effects on niclosamide hydroxylation in HLM (Figure 5). The extent of inhibition rose with an increase in the inhibitor concentration (Figure 5). These results indicated that CYP1A2 was involved in hepatic hydroxylation of niclosamide.

Reaction kinetics for glucuronidation of niclosamide by liver microsomes

Kinetic profiling revealed that glucuronidation of niclosamide in all liver microsomes except RLM followed the classical Michaelis–Menten kinetics (Figure 6). The glucuronidation reaction mediated by RLM showed a biphasic profile that was well described by the biphasic kinetic model (Figure 6). The low K_m value of 1.02 μM and the high CL_{int} value of

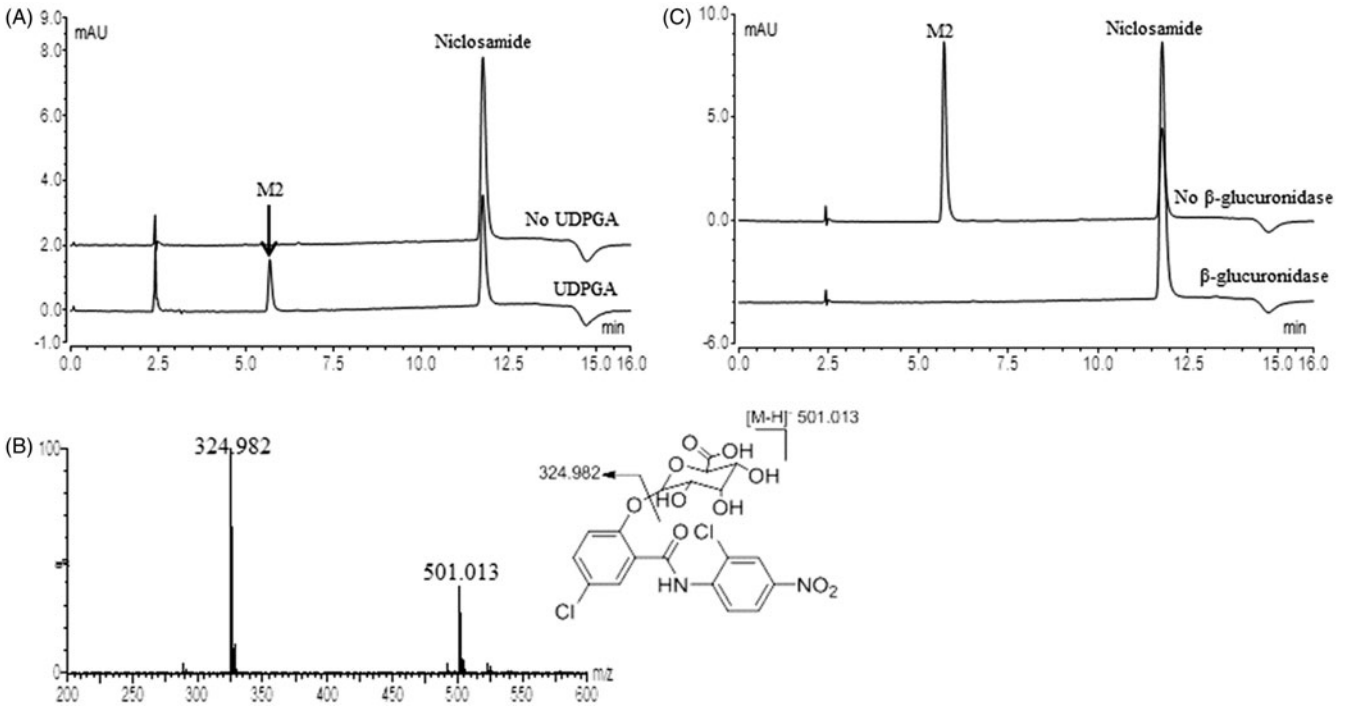

Figure 2. (A) The representative HPLC chromatograms for quantitative analyses of niclosamide and its glucuronide. (B) Structure, MS/MS spectrum and fragmentation pathway of niclosamide glucuronide. (C) Comparisons of HPLC chromatograms, showing that niclosamide glucuronide can be hydrolyzed back to the parent compound (niclosamide) by β-glucuronidase.

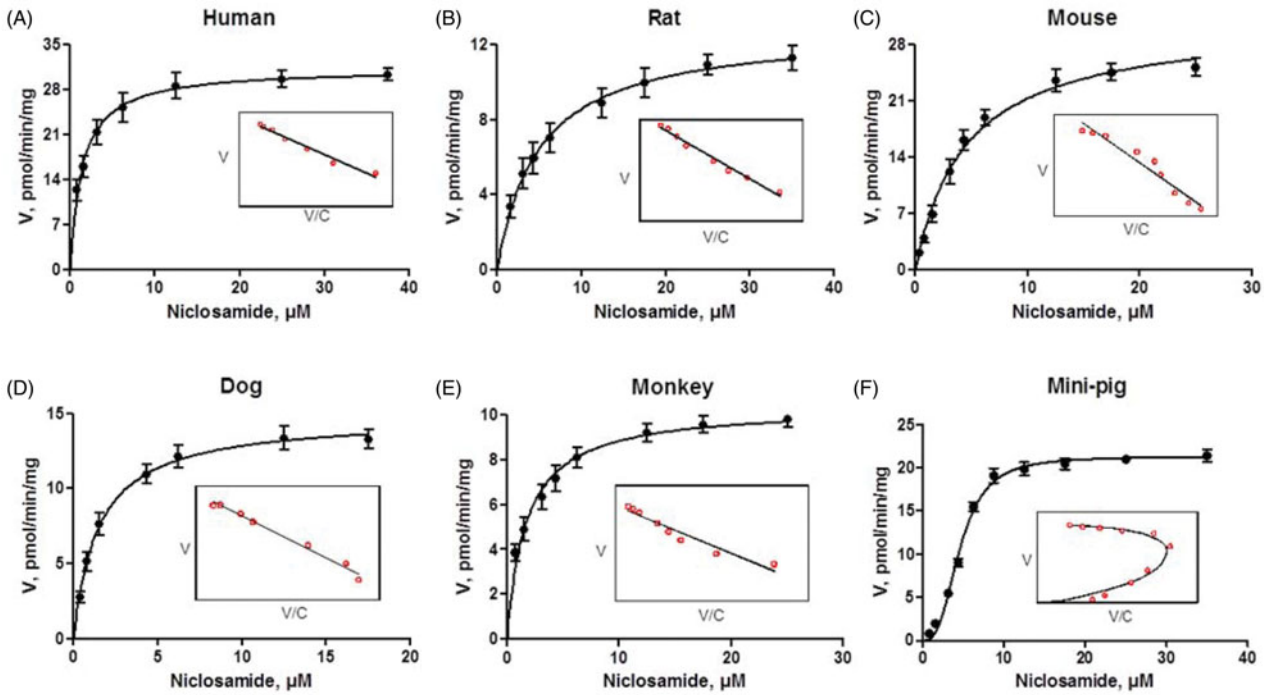

Figure 3. Kinetic profiles for niclosamide hydroxylation by (A) pooled human, (B) rat, (C) mouse, (D) dog, (E) monkey, (F) mini-pig liver microsomes. In each panel, the inset shows the corresponding Eadie–Hofstee plot. Please refer to Table 1 for derived kinetic parameters.

1.36 ml/min/mg suggested that niclosamide was an excellent substrate for UGT metabolism in HLM (Table 2). Marked species differences were also noted for the derived kinetic parameters (Table 2). The K_m values ranged from 0.22 to 2.91 μM; the V_{max} values ranged from 0.09 to 1.38 nmol/min/mg; and the CL_{int} values ranged from 0.12 to 1.36 μl/min/mg. Among animals, monkey showed the glucuronidation parameters that were closest to those of human (Table 2). The kinetic parameters differed by a ≤2.4-fold between monkey and human.

Glucuronidation of niclosamide by expressed UGT enzymes

Of 12 UGT enzymes, seven (i.e., UGT1A1, 1A3, 1A7, 1A8, 1A9, 1A10 and 2B7) generated the glucuronide from

Table 1. Kinetic parameters derived for niclosamide hydroxylation by liver microsomes and expressed CYP enzymes.

Enzymes	V_{max} (pmol/min/mg)	K_m or S_{50} (μM)	K_{si}	n	CL_{int}/CL_{max} (μl/min/mg)	Fitted model
HLM	31.2 ± 0.44	1.38 ± 0.09	NA	NA	22.6 ± 1.52	MM
CYP1A2	7.43 ± 0.40[a]	4.88 ± 0.50	70.2 ± 12.4	NA	1.52 ± 0.18[b]	SI
RLM	12.8 ± 0.22	4.92 ± 0.28	NA	NA	2.61 ± 0.15	MM
MsLM	31.0 ± 1.10	4.51 ± 0.47	NA	NA	6.88 ± 0.76	MM
DLM	21.6 ± 0.53	6.24 ± 0.46	NA	NA	3.46 ± 0.27	MM
PLM	21.3 ± 0.43	4.59 ± 0.58	NA	2.87 ± 0.28	2.43 ± 0.31	Hill
MkLM	10.4 ± 0.25	1.71 ± 0.17	NA	NA	6.07 ± 0.63	MM

Data are represented by mean ± SD. HLM, human liver microsomes; DLM, dog liver microsomes; PLM, mini-pig liver microsomes; MkLM, monkey liver microsomes; MsLM, mouse liver microsomes; RLM, rat liver microsomes; NA, not applicable; MM, Michaelis–Menten model; SI, substrate inhibition.
[a]The unit was nmol/min/nmol.
[b]The unit was ml/min/nmol.

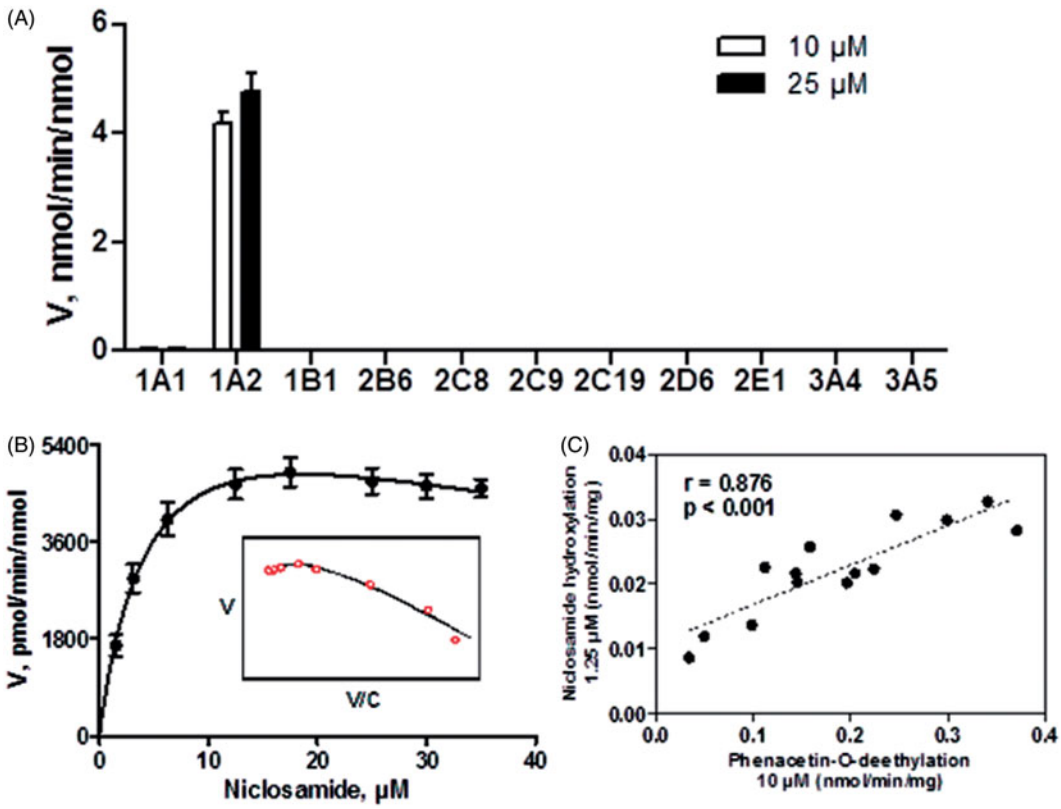

Figure 4. (A) Rate comparisons of niclosamide hydroxylation by 10 expressed CYP enzymes. (B) Kinetic profile for hydroxylation of niclosamide by expressed CYP1A2, the inset shows the corresponding Eadie–Hofstee plot. (C) Correlation analysis between niclosamide hydroxylation and phenacetin deethylation in a bank of individual HLMs ($n = 14$).

niclosamide (Figure 7). Glucuronidation of niclosamide by the seven UGT enzymes displayed the substrate inhibition (for UGT1A1 and 1A3) or Michaelis–Menten (for UGT1A7, 1A8, 1A9, 1A10 and 2B7) profiles (Figure 7). Based on a comparison of the apparent CL_{int} values (Figure 8A), UGT1A1 was the most active enzyme in glucuronidating niclosamide, followed by UGT1A3 and 1A8. UGT1A1 showed the highest CL_{int} value of 8.34 ml/min/mg and lowest K_m value of 0.16 μM. By contrast, glucuronidation of niclosamide by UGT1A3, 1A7, 1A8, 1A9, 1A10, and 2B7 was less efficient with much lower CL_{int} values of 0.04–0.75 ml/min/mg as well as much higher K_m values of 0.77–4.15 μM (Table 2). The results suggested that UGT1A1 may be a main enzyme contributing to glucuronidation of niclosamide.

Activity correlation analyses for UGT1A1

Glucuronidation of β-estradiol (3-OH) is a well-accepted functional marker for UGT1A1 (Court, 2005). We measured the glucuronidation activities of individual HLMs ($n = 14$) toward β-estradiol (3-OH). The rates of niclosamide glucuronidation in the same bank of individual HLMs were also determined. It was found that glucuronidation of niclosamide at 1.25 μM was strongly correlated with 3-*O*-glucuronidation of β-estradiol ($r = 0.888$, $p < 0.001$)

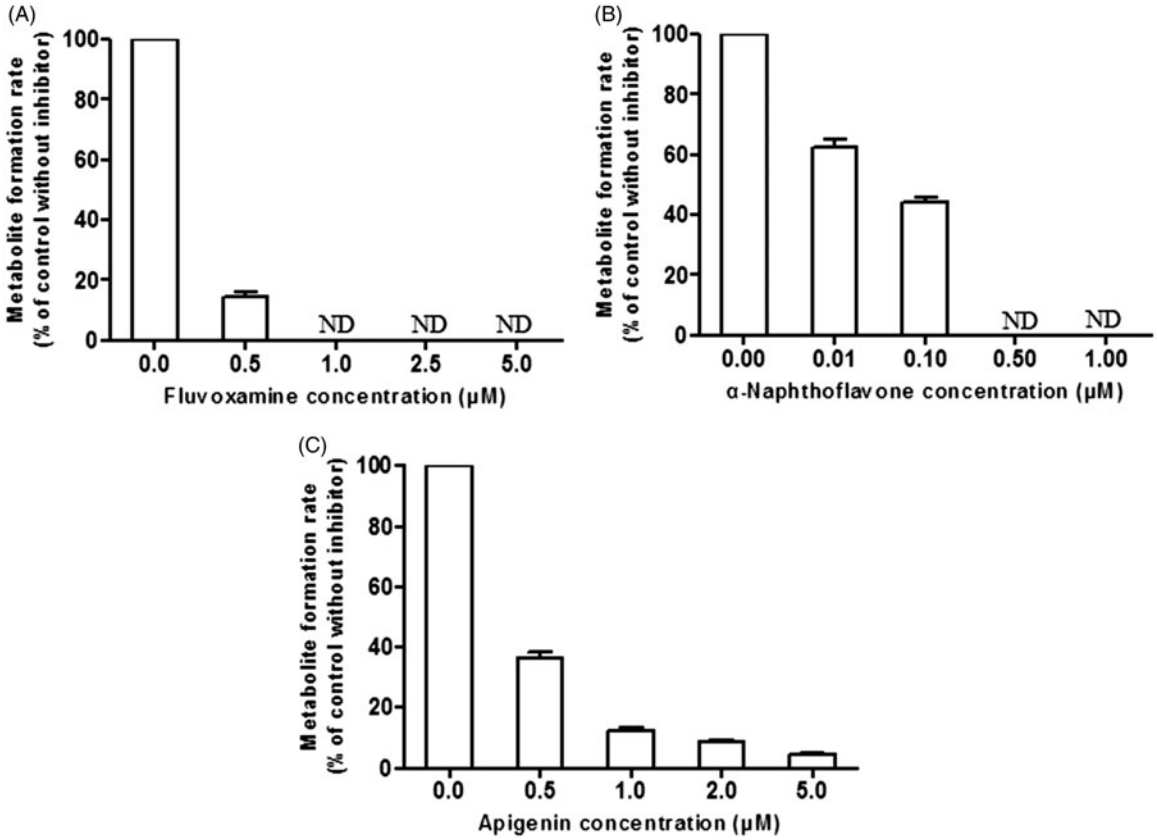

Figure 5. Concentration-dependent inhibition effects of fluvoxamine (A), α-naphthoflavone (B) and apigenin (C) on the catalytic activity of niclosamide hydroxylation by CYP1A2 in pHLM.

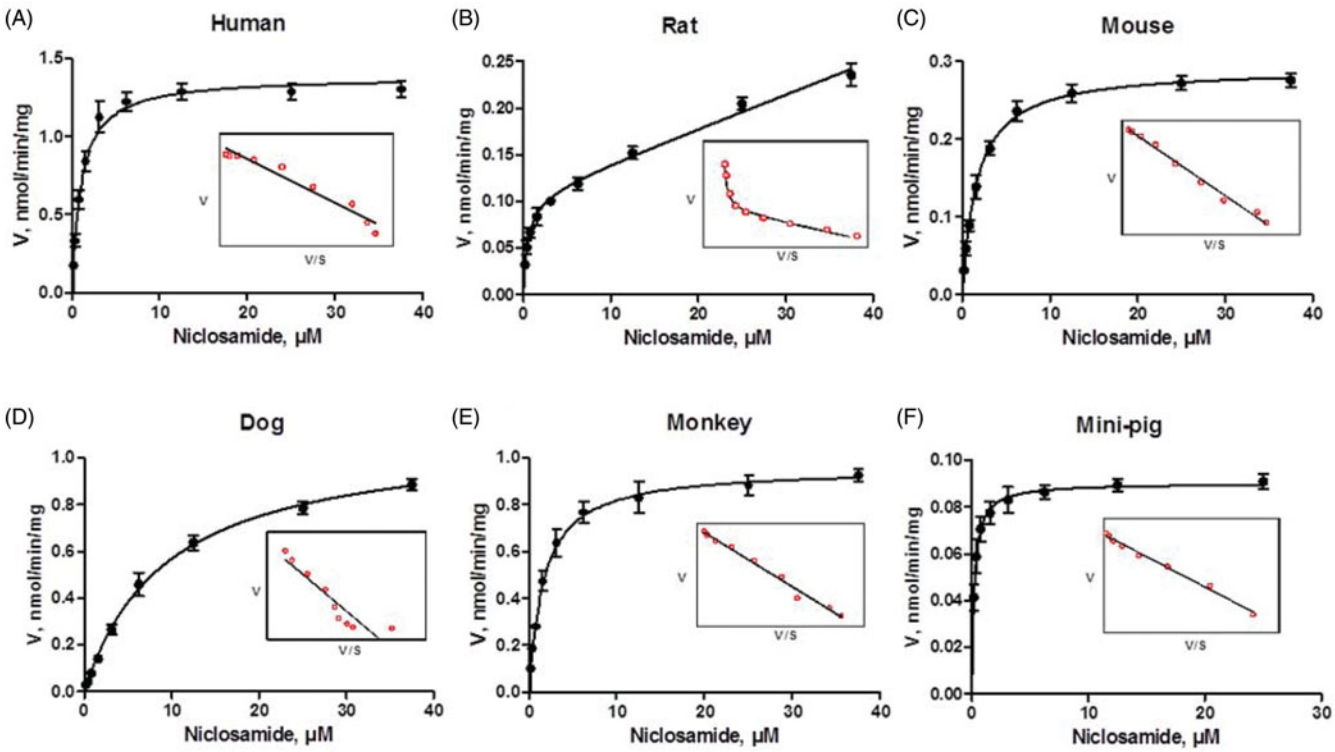

Figure 6. Kinetic profiles for niclosamide glucuronidation by (A) pooled human, (B) rat, (C) mouse, (D) dog, (E) monkey, (F) mini-pig liver microsomes. In each panel, the inset shows the corresponding Eadie–Hofstee plot. Please refer to Table 2 for derived kinetic parameters.

Table 2. Kinetic parameters derived for niclosamide glucuronidation by liver microsomes and expressed UGT enzymes.

Enzymes	V_{max} (nmol/min/mg)	K_m (μM)	K_{si}	CL_{int} (ml/min/mg)	Fitted model
HLM	1.38 ± 0.03	1.02 ± 0.10	NA	1.36 ± 0.14	MM
UGT1A1	1.32 ± 0.29	0.16 ± 0.08	2.70 ± 1.33	8.34 ± 2.30	SI
UGT1A3	1.34 ± 0.25	1.79 ± 0.71	28.1 ± 12.8	0.75 ± 0.17	SI
UGT1A7	0.10 ± 0.01	0.91 ± 0.11	NA	0.11 ± 0.01	MM
UGT1A8	0.65 ± 0.02	1.10 ± 0.17	NA	0.59 ± 0.09	MM
UGT1A9	0.09 ± 0.01	0.77 ± 0.12	NA	0.12 ± 0.02	MM
UGT1A10	0.14 ± 0.01	1.22 ± 0.16	NA	0.11 ± 0.01	MM
UGT2B7	0.18 ± 0.01	4.15 ± 0.20	NA	0.04 ± 0.00	MM
RLM	0.11 ± 0.01	0.51 ± 0.09	NA	0.22 ± 0.04	Biphasic
MsLM	0.29 ± 0.01	1.67 ± 0.06	NA	0.18 ± 0.01	MM
DLM	1.10 ± 0.02	9.39 ± 0.50	NA	0.12 ± 0.01	MM
PLM	0.09 ± 0.01	0.22 ± 0.01	NA	0.40 ± 0.02	MM
MkLM	0.96 ± 0.01	1.66 ± 0.07	NA	0.58 ± 0.03	MM

Data are represented by mean ± SD. HLM, human liver microsomes; DLM, dog liver microsomes; PLM, mini-pig liver microsomes; MkLM, monkey liver microsomes; MsLM, mouse liver microsomes; RLM, rat liver microsomes; NA, not applicable; MM, Michaelis–Menten model; SI, substrate inhibition.

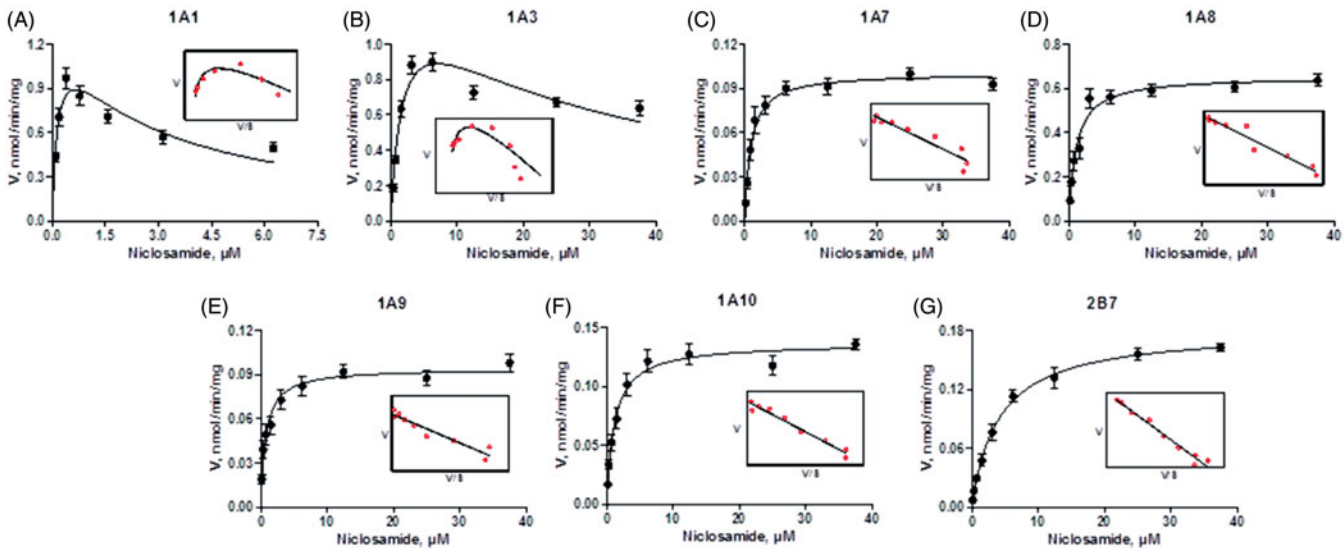

Figure 7. Kinetic profiles for niclosamide glucuronidation by expressed (A) UGT1A1, (B) UGT1A3, (C) UGT1A7, (D) UGT1A8, (E) UGT1A9, (F) UGT1A10, (G) UGT2B7. In each panel, the inset shows the corresponding Eadie–Hofstee plot. Please refer to Table 2 for derived kinetic parameters.

(Figure 8B). Glucuronidation of niclosamide at 2.5 μM was also significantly correlated with 3-*O*-glucuronidation of β-estradiol ($r = 0.809$, $p < 0.001$) (Figure 8C). The results indicated that UGT1A1 played a critical role in niclosamide glucuronidation.

In a similar manner, we performed the correlation analysis between glucuronidation of niclosamide (1.25–2.5 μM) and 24-acyl-glucuronidation of chenodeoxycholic acid (10 μM). There was no significant correlation between niclosamide glucuronidation and chenodeoxycholic acid 24-acyl-glucuronidation ($r \leq 0.07$, $p \geq 0.815$) (Figure 8D and E). This suggested that contribution of UGT1A3 to hepatic glucuronidation of niclosamide was none or negligible.

Discussion

By using microsomal incubations, this study for the first time elucidated the metabolic pathways of niclosamide, an old anthelmintic drug. The chemical structures of metabolites were rigorously determined by high-resolution mass spectrometry and/or NMR analysis. It was found that niclosamide was subjected to efficient hydroxylation and glucuronidation. Furthermore, a combined approach of reaction phenotyping and activity correlation analysis was utilized to identify the main enzymes contributing to hepatic metabolism of niclosamide. The results consistently showed that CYP1A2 and UGT1A1 were the main contributors to niclosamide hydroxylation and glucuronidation, respectively. It was noteworthy that the enzyme activities here were not corrected for the ''albumin effect'' that arose from the fatty acid competition for metabolism (Manevski et al., 2011; Rowland et al., 2008). This may result in an uncertainty in comparing the enzyme catalysis (Figures 4 and 8). Due to a high rate of success in prediction of *in vivo* metabolism using microsomal data (Cubitt et al., 2011; Gertz et al., 2011; Hallifax et al., 2010; Wu et al., 2013), our study should be very helpful for a better understanding of *in vivo* disposition of niclosamide.

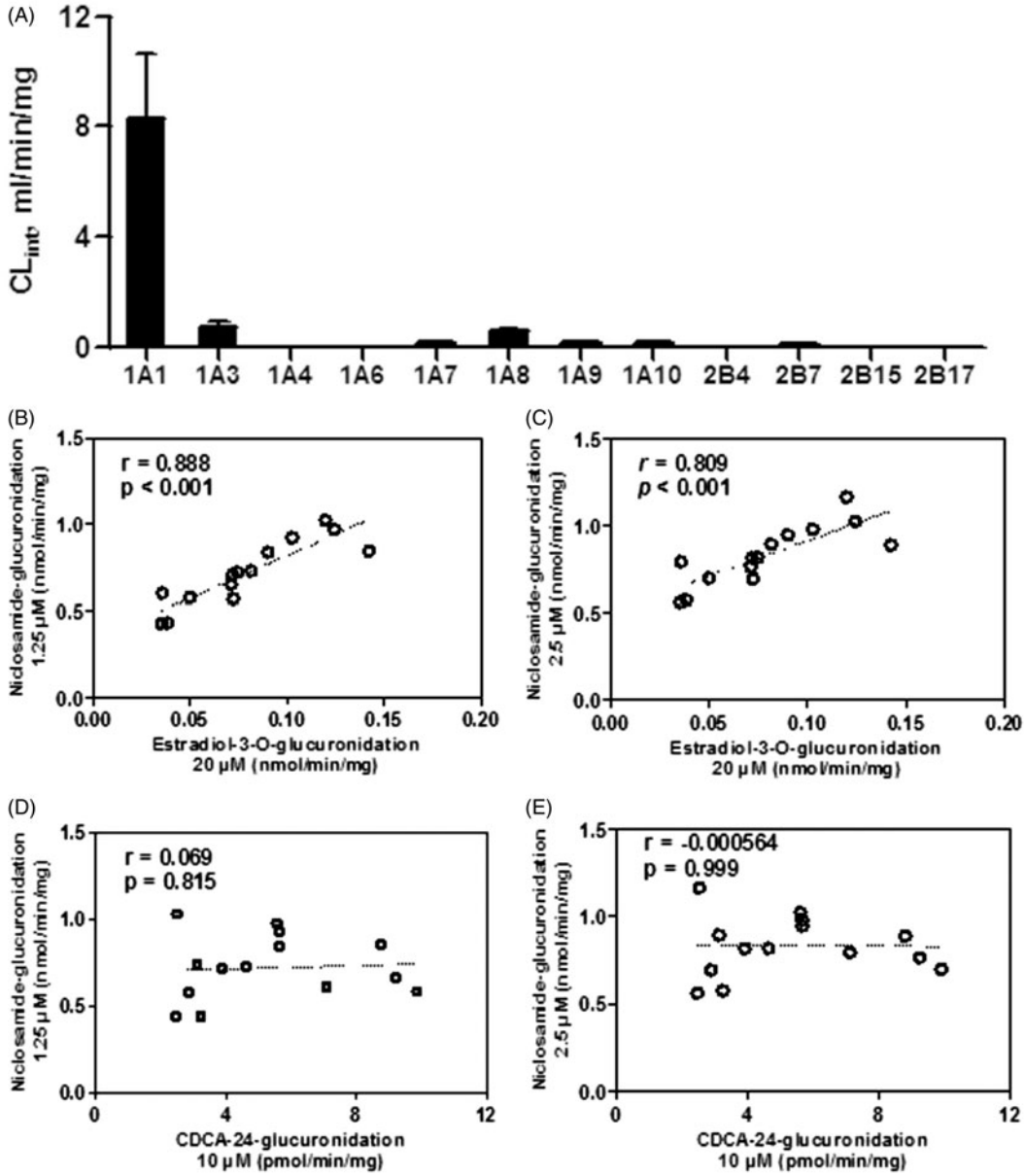

Figure 8. (A) Comparisons of the intrinsic values (CL_{int}) for niclosamide glucuronidation by 12 expressed UGT enzymes. (B and C) Correlation analysis between niclosamide glucuronidation and estradiol glucuronidation in a bank of individual HLMs ($n = 14$). (D and E) Correlation analysis between niclosamide glucuronidation and chenodeoxycholic acid glucuronidation in a bank of individual HLMs ($n = 14$).

We found that UGT1A1 was primarily responsible for glucuronidation of niclosamide in the liver and glucuronidation of niclosamide occurred at the phenolic hydroxyl group. In our previous studies and others, UGT1A1 contributed significantly to hepatic glucuronidation of the compounds bearing hydroxyl group(s) such as macelignan and capsaicin (Liu et al., 2014a; Sun et al., 2014; Wang et al., 2013). Hence, the role of UGT1A1 in glucuronidation of drugs containing hydroxyl group(s) should never be underestimated. In addition, UGT1A1 is a polymorphic enzyme. The UGT1A1 polymorphism (UGT1A1*28) has been associated with the dose-limiting toxicities in irinotecan (also known as CPT-11) chemotherapy (Fujita & Sparreboom, 2010; Nagar & Blanchard, 2006). Thus, varied glucuronidation of niclosamide would be highly possible among UGT1A1 genotypes. However, it remained to be investigated whether the overall metabolism and drug exposure of niclosamide would be influenced by the UGT1A1 polymorphisms.

Metabolic activities of the enzymes toward niclosamide were determined by kinetic profiling that included the metabolic rates at various substrate concentrations. Comparisons of enzyme activities were performed based on the parameter CL_{int} (intrinsic clearance) derived from kinetic modeling. The CL_{int} value, independent of substrate concentration, measures the catalytic efficiency of functional enzymes. Use of CL_{int} was more advantageous in characterization of enzyme activities compared to the metabolic rates (at one or more substrate concentrations). It was noteworthy that the substrate concentrations in microsomal incubations (and the kinetic parameters) were not corrected by protein binding. This was because binding of niclosamide ($\log P = 4.0$) to microsomal proteins was negligible

(fu = 97.5) according to the Hallifax and Houston model (Hallifax & Houston, 2006; Zhou et al., 2010). The model consisting of log *P* and microsomal protein concentration has been shown to provide accurate predictions on fu values for the compounds with intermediate lipophilicity (log *P* = 2.5–5) (Gao et al., 2010). Also, comparative assessment of several predictive models of fu has revealed that the Halifax and Houston model is one of the best performing prediction methods (Poulin & Haddad, 2011).

Systemic bioavailability of niclosamide was very low after oral uptake of the drug (~10% in rats) (Chang et al., 2006). Oral niclosamide is effective in management of tapeworms that resides in the intestinal lumen (Al-Hadiya, 2005). However, the low systemic bioavailability may be a concern when it comes to the chemotherapy with niclosamide wherein the intestinal lumen is not the target site. A better understanding of the causes to poor intestinal absorption of niclosamide would help to find means to enhance the oral bioavailability. Our study indicated that first-pass metabolism in the liver and intestine would be a significant limiting factor to oral absorption of niclosamide. Although the metabolism data were unavailable with intestine microsomes, there is a high possibility that niclosamide would be subjected to intestinal glucuronidation. This is because the human intestine abundantly expresses the catalytically active UGT enzymes (e.g., UGT1A1, 1A8, 1A10 and 2B7) (Nakamura et al., 2008; Ohno & Nakajin, 2009). Intestinal hydroxylation should be negligible or none because CYP1A2 is not expressed in human intestine (Paine et al., 2006).

In an early study, a reduced metabolite was generated from niclosamide by mouse liver homogenate (Douch & Gahagan, 1977). However, no such metabolite was found in our microsomal incubations (mouse and all other species). This inconsistency may be accounted for by the differences in enzyme sources. It was speculated that the reduction reaction was catalyzed by the enzymes that were not expressed in the microsomal organelles. By contrast, our finding that niclosamide underwent efficient glucuronidation in various animals was consistent with an early study in which the glucuronidated metabolite was found in fish tissues after exposure to niclosamide (Dawson et al., 1999). This may indicate that the glucuronidation reaction was a universal detoxification mechanism for niclosamide among animal species.

Three CYP1A2 inhibitors (i.e., fluvoxamine, α-naphthoflavone and apigenin) were selected to assess their inhibitory effects on niclosamide hydroxylation in HLM. Fluvoxamine is a selective inhibitor of CYP1A2, whereas the other two inhibitors are dual inhibitors of both CYP1A1 and 1A2 (Pastrakuljic et al., 1997; Reid et al., 1999). Inhibition of niclosamide metabolism by α-naphthoflavone (or fluvoxamine) was essentially complete at concentrations of ≥0.5 μM (or ≥1 μM). More than 80% of niclosamide metabolism was inhibited by apigenin at concentrations of ≥1 μM (Figure 5). The results were consistent with previous findings that fluvoxamine, α-naphthoflavone and apigenin were rather potent CYP1A2 inhibitors (Pastrakuljic et al., 1997; Reid et al., 1999).

Hydroxylation of niclosamide mediated by HLM followed Michaelis–Menten kinetics, whereas the reaction mediated by the main active enzyme CYP1A2 displayed substrate inhibition kinetics (Figures 3 and 4). Likewise, glucuronidation of niclosamide mediated by HLM followed Michaelis–Menten kinetics, whereas the reaction mediated by UGT1A1 (the main contributing enzyme) displayed substrate inhibition kinetics (Figures 6 and 7). Similar observations have been also noted in the study of Zhu et al. (2012). Glucuronidation of magnolol by HIM showed substrate inhibition kinetics, but UGT1A10 (one main contributor) displayed Michaelis–Menten kinetics (Zhu et al., 2012). Although we were unable to provide exact explanations for this apparent ''conflict'', the distinct kinetic profiles may be associated with the differences in enzyme sources. HLM or HIM is human tissue specific, whereas the recombinant enzymes were prepared from insect cells overexpressing a particular enzyme.

In conclusion, we have characterized the metabolism of niclosamide by CYP and UGT enzymes using liver microsomes and expressed enzymes. NADPH-supplemented HLM (and liver microsomes from various animal species) generated one hydroxylated metabolite (M1) from niclosamide; and UDPGA-supplemented liver microsomes generated one mono-*O*-glucuronide (M2). The chemical structures of M1 and M2 were determined through LC–MS/MS and/or NMR analyses. Reaction phenotyping revealed that CYP1A2 was the main enzyme responsible for M1 formation. The important role of CYP1A2 in niclosamide metabolism was further confirmed by activity correlation analysis as well as inhibition experiments using specific inhibitors. Although seven UGT enzymes were able to catalyze glucuronidation of niclosamide, UGT1A1 and 1A3 were the enzymes showed the highest metabolic activities. Activity correlation analyses showed that UGT1A1 played a predominant role in hepatic glucuronidation of niclosamide, whereas the role of UGT1A3 was negligible or none. This was the first report that niclosamide was subjected to efficient hydroxylation and glucuronidation, wherein CYP1A2 and UGT1A1 were the main contributing enzymes, respectively.

Declaration of interest

This work was supported by the National Natural Science Foundation of China (No. 81373496), the Program for Pearl River New Stars of Science and Technology in Guangzhou (No. 2014059), and the Doctoral Fund of Ministry of Education of China (20134401120014). The authors report no conflict of interest.

References

Al-Hadiya BM. (2005). Niclosamide: comprehensive profile. Profiles Drug Subst Excip Relat Methodol 32:67–96.

Bjornsson TD, Callaghan JT, Einolf HJ, et al., Pharmaceutical Research and Manufacturers of America (PhRMA) Drug Metabolism/Clinical Pharmacology Technical Working Group; FDA Center for Drug Evaluation and Research (CDER). (2003). The conduct of *in vitro* and *in vivo* drug–drug interaction studies: a Pharmaceutical Research and Manufacturers of America (PhRMA) perspective. Drug Metab Dispos 31:815–32.

Chang YW, Yeh TK, Lin KT, et al. (2006). Pharmacokinetics of anti-SARS-CoV agent niclosamide and its analogs in rats. J Food Drug Anal 14:329–33.

Costa A, Sarmento B, Seabra V. (2014). An evaluation of the latest *in vitro* tools for drug metabolism studies. Expert Opin Drug Metab Toxicol 10:103–19.

Court MH. (2005). Isoform-selective probe substrates for *in vitro* studies of human UDP-glucuronosyltransferases. Methods Enzymol 400: 104–16.

Cubitt HE, Houston JB, Galetin A. (2011). Prediction of human drug clearance by multiple metabolic pathways: integration of hepatic and intestinal microsomal and cytosolic data. Drug Metab Dispos 39: 864–73.

Dawson VK, Schreier TM, Boogaard MA, Gingerich WH. (1999). Uptake, metabolism, and elimination of niclosamide by fish. In: Smith DJ, Gingerich WH, Beconi-Barker MG, eds. Xenobiotics in fish. Springer, 167–76.

Douch PG, Gahagan HM. (1977). The metabolism of niclosamide and related compounds by *Moniezia expansa*, *Ascaris lumbricoides* var suum, and mouse- and sheep-liver enzymes. Xenobiotica 7:301–7.

Emoto C, Murayama N, Rostami-Hodjegan A, Yamazaki H. (2010). Methodologies for investigating drug metabolism at the early drug discovery stage: prediction of hepatic drug clearance and P450 contribution. Curr Drug Metab 11:678–85.

Evans WE, Relling MV. (1999). Pharmacogenomics: translating functional genomics into rational therapeutics. Science 286:487–91.

Fang ZZ, Krausz KW, Nagaoka K, et al. (2014). *In vivo* effects of the pure aryl hydrocarbon receptor antagonist GNF-351 after oral administration are limited to the gastrointestinal tract. Br J Pharmacol 171:1735–46.

Fonseca BD, Diering GH, Bidinosti MA, et al. (2012). Structure–activity analysis of niclosamide reveals potential role for cytoplasmic pH in control of mammalian target of rapamycin complex 1 (mTORC1) signaling. J Biol Chem 287:17530–45.

Fujita K, Sparreboom A. (2010). Pharmacogenetics of irinotecan disposition and toxicity: a review. Curr Clin Pharmacol 5: 209–17.

Gao H, Steyn SJ, Chang G, Lin J. (2010). Assessment of *in silico* models for fraction of unbound drug in human liver microsomes. Expert Opin Drug Metab Toxicol 6:533–42.

Gertz M, Houston JB, Galetin A. (2011). Physiologically based pharmacokinetic modeling of intestinal first-pass metabolism of CYP3A substrates with high intestinal extraction. Drug Metab Dispos 39:1633–42.

Griffiths LA, Facchini V. (1979). The major metabolites of niclosamide: identification by mass spectrometry. In: Frigerio A, ed. Recent developments in mass spectrometry in biochemistry and medicine. Vol. 2. Springer, 121–6.

Hallifax D, Foster JA, Houston JB. (2010). Prediction of human metabolic clearance from *in vitro* systems: retrospective analysis and prospective view. Pharm Res 27:2150–61.

Hallifax D, Houston JB. (2006). Binding of drugs to hepatic microsomes: comment and assessment of current prediction methodology with recommendation for improvement. Drug Metab Dispos 34:724–6; author reply 727.

Hutzler JM, Tracy TS. (2002). Atypical kinetic profiles in drug metabolism reactions. Drug Metab Dispos 30:355–62.

Imperi F, Massai F, Ramachandran Pillai C, et al. (2013). New life for an old drug: the anthelmintic drug niclosamide inhibits *Pseudomonas aeruginosa* quorum sensing. Antimicrob Agents Chemother 57: 996–1005.

Jin Y, Lu Z, Ding K, et al. (2010). Antineoplastic mechanisms of niclosamide in acute myelogenous leukemia stem cells: inactivation of the NF-kappaB pathway and generation of reactive oxygen species. Cancer Res 70:2516–27.

Kassahun K, Mattiuz E, Franklin R, Gillespie T. (1998). Olanzapine 10-*N*-glucuronide: a tertiary *N*-glucuronide unique to humans. Drug Metab Dispos 26:848–55.

Kola I, Landis J. (2004). Can the pharmaceutical industry reduce attrition rates? Nat Rev Drug Discov 3:711–15.

Li Y, Li PK, Roberts MJ, et al. (2014). Multi-targeted therapy of cancer by niclosamide: a new application for an old drug. Cancer Lett 349: 8–14.

Liu W, Liu H, Sun H, et al. (2014b). Metabolite elucidation of the Hsp90 inhibitor SNX-2112 using ultraperformance liquid chromatography/quadrupole time-of-flight mass spectrometry (UPLC-QTOF/MS). Xenobiotica 44:455–64.

Liu H, Sun H, Lu D, et al. (2014a). Identification of glucuronidation and biliary excretion as the main mechanisms for gossypol clearance: *in vivo* and *in vitro* evidence. Xenobiotica 44:696–707.

Mackenzie PI, Bock KW, Burchell B, et al. (2005). Nomenclature update for the mammalian UDP glycosyltransferase (UGT) gene superfamily. Pharmacogenet Genomics 15:677–85.

Manevski N, Moreolo PS, Yli-Kauhaluoma J, Finel M. (2011). Bovine serum albumin decreases Km values of human UDP-glucuronosyltransferases 1A9 and 2B7 and increases Vmax values of UGT1A9. Drug Metab Dispos 39:2117–29.

Nagar S, Blanchard RL. (2006). Pharmacogenetics of uridine diphosphoglucuronosyltransferase (UGT) 1A family members and its role in patient response to irinotecan. Drug Metab Rev 38: 393–409.

Nakajima M, Nakamura S, Tokudome S, et al. (1999). Azelastine *N*-demethylation by cytochrome P-450 (CYP)3A4, CYP2D6, and CYP1A2 in human liver microsomes: evaluation of approach to predict the contribution of multiple CYPs. Drug Metab Dispos 27: 1381–91.

Nakamura A, Nakajima M, Yamanaka H, et al. (2008). Expression of UGT1A and UGT2B mRNA in human normal tissues and various cell lines. Drug Metab Dispos 36:1461–4.

Ohno S, Nakajin S. (2009). Determination of mRNA expression of human UDP-glucuronosyltransferases and application for localization in various human tissues by real-time reverse transcriptase-polymerase chain reaction. Drug Metab Dispos 37:32–40.

Ortiz de Montellano PR. (2005). Cytochrome P450: structure, mechanism, and biochemistry. Springer Science & Business Media.

Paine MF, Hart HL, Ludington SS, et al. (2006). The human intestinal cytochrome P450 ''pie''. Drug Metab Dispos 34:880–6.

Pan JX, Ding K, Wang CY. (2012). Niclosamide, an old antihelminthic agent, demonstrates antitumor activity by blocking multiple signaling pathways of cancer stem cells. Chin J Cancer 31:178–84.

Park SJ, Shin JH, Kang H, et al. (2011). Niclosamide induces mitochondria fragmentation and promotes both apoptotic and autophagic cell death. BMB Rep 44:517–22.

Pastrakuljic A, Tang BK, Roberts EA, Kalow W. (1997). Distinction of CYP1A1 and CYP1A2 activity by selective inhibition using fluvoxamine and isosafrole. Biochem Pharmacol 53:531–8.

Poulin P, Haddad S. (2011). Microsome composition-based model as a mechanistic tool to predict nonspecific binding of drugs in liver microsomes. J Pharm Sci 100:4501–17.

Prentis RA, Lis Y, Walker SR. (1988). Pharmaceutical innovation by the seven UK-owned pharmaceutical companies (1964–1985). Br J Clin Pharmacol 25:387–96.

Reid JM, Kuffel MJ, Miller JK, et al. (1999). Metabolic activation of dacarbazine by human cytochromes P450: the role of CYP1A1, CYP1A2, and CYP2E1. Clin Cancer Res 5: 2192–7.

Rowland A, Elliot DJ, Knights KM, et al. (2008). The ''albumin effect'' and *in vitro–in vivo* extrapolation: sequestration of long-chain unsaturated fatty acids enhances phenytoin hydroxylation by human liver microsomal and recombinant cytochrome P450 2C9. Drug Metab Dispos 36:870–7.

Seo KA, Kim HJ, Jeong ES, et al. (2014). *In vitro* assay of six UDP-glucuronosyltransferase isoforms in human liver microsomes, using cocktails of probe substrates and liquid chromatography–tandem mass spectrometry. Drug Metab Dispos 42:1803–10.

Shet MS, McPhaul M, Fisher CW, et al. (1997). Metabolism of the antiandrogenic drug (Flutamide) by human CYP1A2. Drug Metab Dispos 25:1298–303.

Shimada H, Eto M, Ohtaguro M, et al. (2010). Differential mechanisms for the inhibition of human cytochrome P450 1A2 by apigenin and genistein. J Biochem Mol Toxicol 24:230–4.

Sun H, Wang H, Liu H, et al. (2014). Glucuronidation of capsaicin by liver microsomes and expressed UGT enzymes: reaction kinetics, contribution of individual enzymes and marked species differences. Expert Opin Drug Metab Toxicol 10:1325–36.

Tassaneeyakul W, Birkett DJ, Veronese ME, et al. (1993). Specificity of substrate and inhibitor probes for human cytochromes P450 1A1 and 1A2. J Pharmacol Exp Ther 265:401–7.

von Moltke LL, Weemhoff JL, Bedir E, et al. (2004). Inhibition of human cytochromes P450 by components of *Ginkgo biloba*. J Pharm Pharmacol 56:1039–44.

Wang AM, Ku HH, Liang YC, et al. (2009). The autonomous notch signal pathway is activated by baicalin and baicalein but is suppressed by niclosamide in K562 cells. J Cell Biochem 106:682–92.

Wang LZ, Ramirez J, Yeo W, et al. (2013). Glucuronidation by UGT1A1 is the dominant pathway of the metabolic disposition of belinostat in liver cancer patients. PLoS One 8:e54522.

Wells PG, Mackenzie PI, Chowdhury JR, et al. (2004). Glucuronidation and the UDP-glucuronosyltransferases in health and disease. Drug Metab Dispos 32:281–90.

Wu B, Dong D, Hu M, Zhang S. (2013). Quantitative prediction of glucuronidation in humans using the *in vitro–in vivo* extrapolation approach. Curr Top Med Chem 13:1343–52.

Zhou J, Tracy TS, Remmel RP. (2010). Glucuronidation of dihydrotestosterone and trans-androsterone by recombinant UDP-glucuronosyltransferase (UGT) 1A4: evidence for multiple UGT1A4 aglycone binding sites. Drug Metab Dispos 38: 431–40.

Zhou SF, Yang LP, Zhou ZW, et al. (2009). Insights into the substrate specificity, inhibitors, regulation, and polymorphisms and the clinical impact of human cytochrome P450 1A2. AAPS J 11:481–94.

Zhu LL, Ge GB, Zhang HB, et al. (2012). Characterization of hepatic and intestinal glucuronidation of magnolol: application of the relative activity factor approach to decipher the contributions of multiple UDP-glucuronosyltransferase isoforms. Drug Metab Dispos 40: 529–38.

Supplementary material available online

Supplementary Tables S1–S3.